nature biotechnology

Protein-retention expansion microscopy of cells and tissues labeled using standard fluorescent proteins and antibodies

Paul W Tillberg[1,2,10], Fei Chen[2,3,10], Kiryl D Piatkevich[2], Yongxin Zhao[2], Chih-Chieh (Jay) Yu[2,3], Brian P English[4], Linyi Gao[3], Anthony Martorell[5], Ho-Jun Suk[2,6], Fumiaki Yoshida[7,8], Ellen M DeGennaro[5,8], Douglas H Roossien[9], Guanyu Gong[3], Uthpala Seneviratne[3], Steven R Tannenbaum[3], Robert Desimone[5,8], Dawen Cai[9] & Edward S Boyden[2,3,5,8]

Expansion microscopy (ExM) enables imaging of preserved specimens with nanoscale precision on diffraction-limited instead of specialized super-resolution microscopes. ExM works by physically separating fluorescent probes after anchoring them to a swellable gel. The first ExM method did not result in the retention of native proteins in the gel and relied on custom-made reagents that are not widely available. Here we describe protein retention ExM (proExM), a variant of ExM in which proteins are anchored to the swellable gel, allowing the use of conventional fluorescently labeled antibodies and streptavidin, and fluorescent proteins. We validated and demonstrated the utility of proExM for multicolor super-resolution (~70 nm) imaging of cells and mammalian tissues on conventional microscopes.

We recently developed a technology, ExM, which enables imaging of thick preserved specimens with ~70 nm lateral resolution[1]. Using ExM, the optical diffraction limit is circumvented via physical expansion of a biological specimen before imaging, thus bringing subdiffraction-limited structures into the size range viewable by a conventional diffraction-limited microscope. We had demonstrated that ExM can be used to image biological specimens at the voxel rates of a diffraction-limited microscope but with the voxel sizes of a super-resolution microscope. Expanded samples are transparent, and index-matched to water, as the expanded material is >99% water. The original ExM protocol involves labeling biomolecules of interest with a gel-anchorable fluorophore. Then, a swellable polyelectrolyte gel is synthesized in the sample, so that it incorporates the labels. Finally, the sample is treated with a nonspecific protease to homogenize its mechanical properties, followed by dialysis in water to mediate uniform physical expansion of the polymer-specimen composite. All of the chemicals required for ExM can be purchased except

for the gel-anchorable label, which requires custom synthesis and raises the barrier for researchers to adopt the method. Another drawback of the ExM protocol is that genetically encoded fluorophores cannot be imaged without antibody labeling.

Here we report the development of a variant of ExM, proExM, in which proteins, rather than labels, are anchored to the swellable gel, using a commercially available cross-linking molecule. We demonstrate that fluorescence signals from genetically encoded fluorescent proteins (FPs) as well as conventional fluorescently labeled secondary antibodies and streptavidin that are directly anchored to the gel are preserved even when subjected to the nonspecific proteolytic digestion from the original ExM protocol. proExM is a simple extension of standard histological methods used to prepare samples for imaging that should enable its adoption.

Strong protease digestion (i.e., with proteinase K) enables isotropic expansion in the original ExM protocol. We asked whether native proteins could be chemically anchored to the ExM gel and stained with antibodies in the expanded state. As a first experiment, we used a modified approach with reduced proteolysis to preserve epitopes. To incorporate proteins into the polymeric gel, we used the succinimidyl ester of 6-((acryloyl)amino)hexanoic acid (acryloyl-X, SE; abbreviated AcX; Life Technologies), which modifies amines on proteins with an acrylamide functional group. Borrowing from denaturing SDS-PAGE[2] and antigen retrieval protocols[3], we treated gel-embedded tissues in an alkaline detergent-rich buffer for 1 h in an autoclave, and found ~4 × expansion of Thy1-YFP mouse brain samples (we imaged endogenous YFP before treatment and labeling after expansion with anti-GFP; **Supplementary Fig. 1a,b**). We found that antibodies could indeed be delivered after expansion (**Supplementary Fig. 1c–e**). As a second treatment strategy, we exposed gel-embedded tissues to LysC, which cuts proteins at lysine residues (in contrast to nonspecific proteinase K)[4,5] (**Supplementary**

Fig. 2). Post-expansion staining in both cases was highly variable depending on antibody identity (for example, compare lamin A/C examined with three different protocols (**Supplementary Fig. 1f**)

to images obtained in the original ExM protocol (supplementary Fig. 4 in ref. 1); additional examples are shown in **Supplementary Fig. 3**). For some antibodies, post-expansion staining appeared to
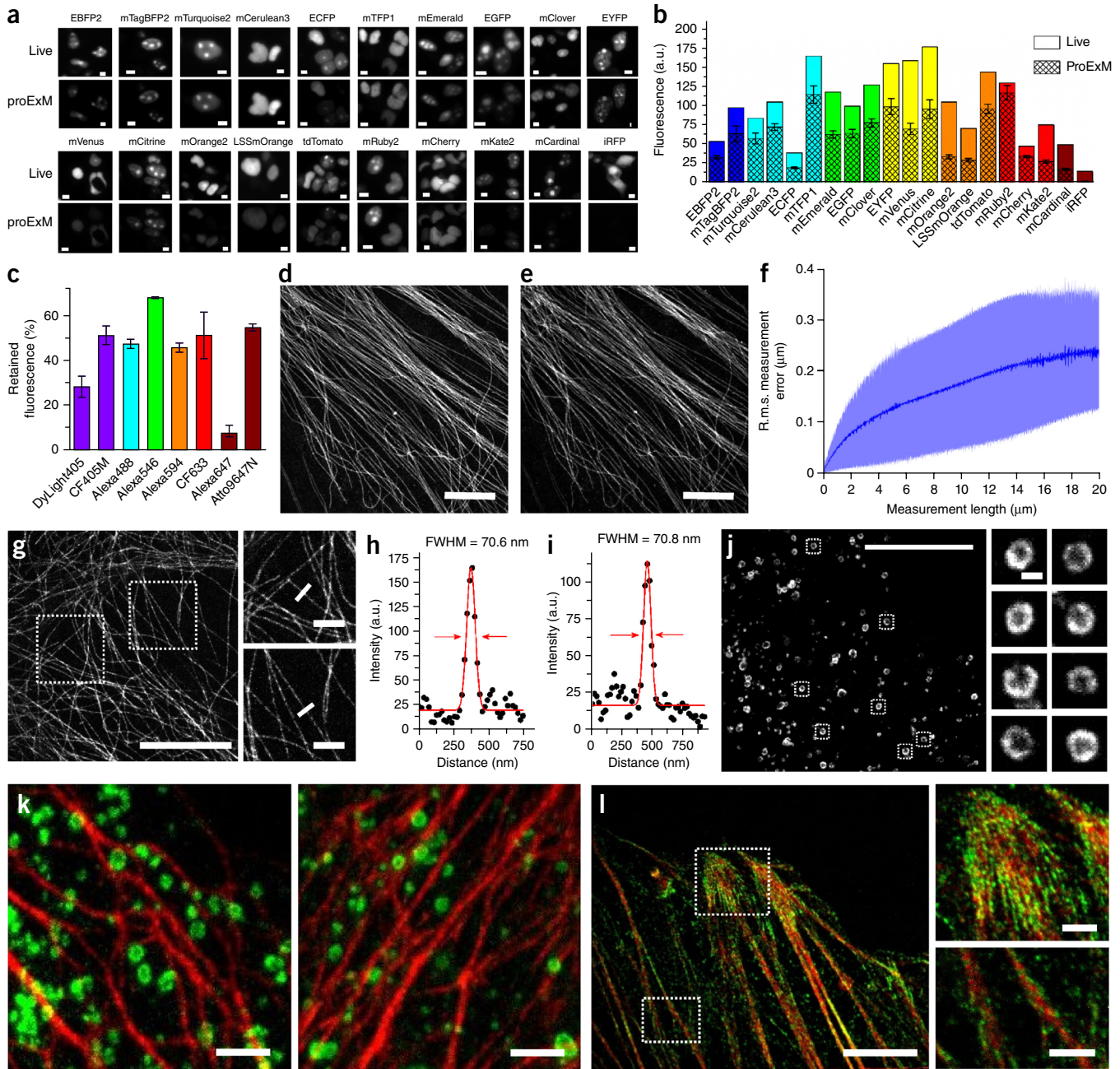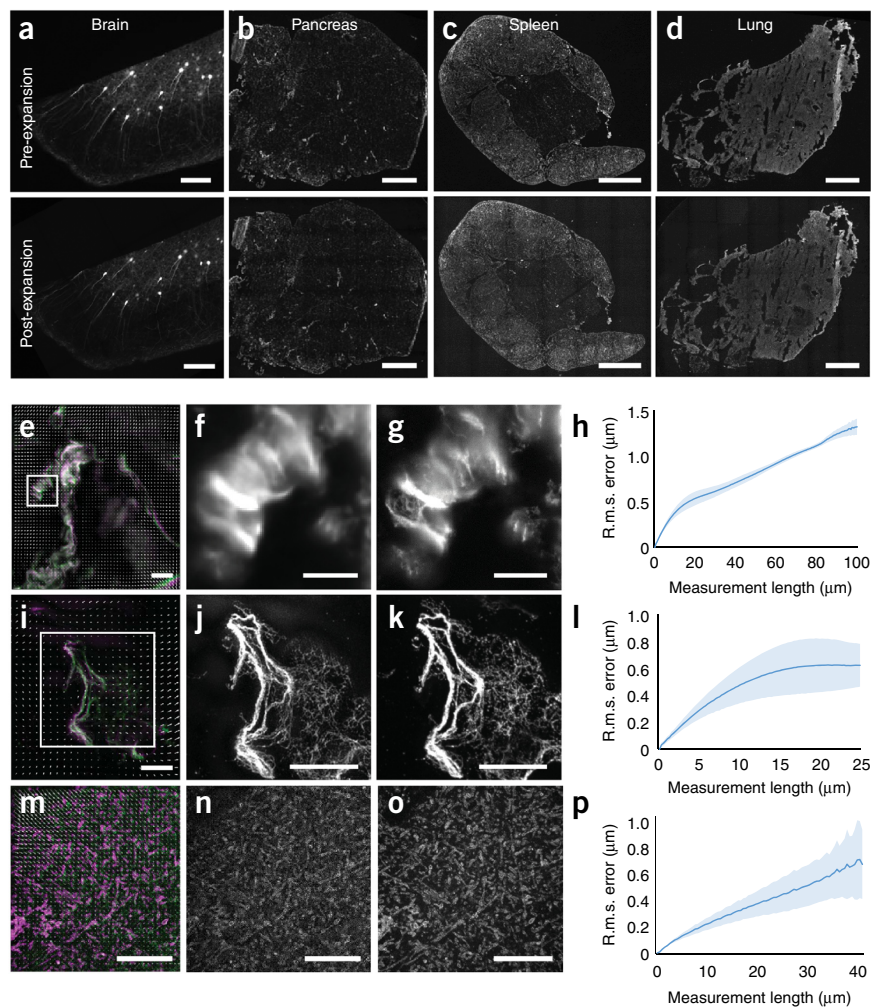
Figure 1 Retention of FP and antibody fluorescence signals in proExM and proExM of FP fusions. (**a**) Representative images of indicated FPs fused to histone proteins in live HEK293FT cells and in the same cells after proExM treatment; iRFP was expressed as N-terminal fusion with nuclear localization sequence (NLS). (**b**) Quantified fluorescence for experiments as in **a**, after proExM treatment (mean ± s.d.; $n = 4$ transfection replicates each). Open bars, literature values of the brightness of these fluorophores, normalized to that of EGFP; literature values are used to avoid confounds due to differential expression, dependent on the user's application, of different fluorophores. Crosshatched bars, literature values of brightness multiplied by the observed retention fraction for each fluorophore (e.g., the ratio of proExM and live, as in **a**). (**c**) Retention of fluorescence for selected dyes conjugated with antibodies, after proExM treatment (mean ± s.d., $n = 3$ samples each), in mouse brain slice. (**d,e**) SR-SIM image of immunostained microtubules after the anchoring step (**d**) and post-expansion image of the same sample acquired with a spinning disk confocal microscope (**e**). (**f**) R.m.s. length measurement error as a function of measurement length for proExM vs. SIM images (blue line, mean; shaded area, s.d.; $n = 4$ samples). (**g**) Confocal image of mClover-α-tubulin fusion. HeLa cells were used in the rest of this figure. Insets show magnified views of boxed regions in **g**. (**h,i**) Quantification of line cuts in **g**. Solid red lines indicate the Gaussian fit used to determine the FWHM (red arrows). (**j**) Confocal image of mEmerald-clathrin fusion (left) and magnified views of single CCPs in the boxed regions (right). (**k**) Dual-color proExM of clathrin (fused to mEmerald, green) and keratin (mRuby2, red); two representative images are shown. (**l**) Dual-color proExM image of actin (mRuby2, red) and paxillin (mEmerald, green) fusions. Insets are magnified views of boxed regions. Scale bars: (**a**) 5 µm, (**d**) 5 µm, (**e**) 5 µm (physical size post-expansion, 20.5 µm); (**g**) 5 µm (21.5 µm) and 1 µm in insets; (**j**) 10 µm (42.6 µm) and 200 nm in insets; (**k**) 1 µm (4.3 µm), (**l**) 5 µm (21.5 µm) and 1 µm in insets.

Figure 2 Validation of proExM in different mammalian tissue types. (**a**–**d**) Low-magnification, widefield images of pre-expansion and post-expansion samples of *Thy1-YFP* mouse brain (**a**), and vimentin-immunostained mouse pancreas (**b**), spleen (**c**) and lung (**d**). (**e**) High-magnification, widefield fluorescence composite image of vimentin in mouse pancreas before (green) and after (purple) expansion with distortion vector field overlaid (white arrows; Online Methods). (**f**,**g**) Pre-expansion widefield image (**f**) and post-expansion image (**g**) of the boxed region in **e**. (**h**) R.m.s. length measurement error as a function of measurement length for proExM vs. widefield pre-expansion images for the different tissue types in **b**–**d** (blue line, mean; shaded area, s.d.; $n = 3$ samples, from pancreas, spleen, and lung). (**i**) Composite fluorescence image of vimentin in mouse pancreas imaged with SR-SIM (green) and proExM (purple) with conventional confocal microscopy with distortion vector field overlaid (white arrows). (**j**,**k**) Pre-expansion SR-SIM image (**j**) and post-expansion confocal image (**k**) of the boxed region in **i**. (**l**) R.m.s. length measurement error as a function of measurement length for proExM vs. SR-SIM pre-expansion for vimentin staining in the pancreas (blue line, mean; shaded area, s.d.; $n = 4$ fields of view from two samples). (**m**) Composite fluorescence image of Tom20 in *Thy1-YFP* mouse brain imaged with SR-SIM (green) and proExM (purple) with conventional confocal microscopy with distortion vector field overlaid (white arrows). (**n**,**o**) Pre-expansion SR-SIM image (**n**) and post-expansion confocal image (**o**) used in **m**. The specimen imaged here is a representative example of the three specimens used in **p**. (**p**) R.m.s. length measurement error as a function

of measurement length for proExM vs. SR-SIM pre-expansion for Tom20 staining in *Thy1-YFP* mouse brain (blue line, mean; shaded area, s.d.; $n = 3$ mouse brain cortex samples). Scale bars: (**a**) 200 μm (physical size post-expansion, 800 μm), (**b**–**d**) 500 μm (2.21 mm, 2.06 mm, 2.04 mm, respectively), (**m**,**n**) 10 μm, (**o**) 10 μm (40 μm), (**e**) 10 μm, (**f**) 5 μm, (**g**) 5 μm (20.4 μm), (**i**,**j**) 5 μm, (**k**) 5 μm (20.65 μm).

result in brighter signal compared to pre-gelation staining (Tom20, GFP and PSD-95; **Supplementary Fig. 1g,h**). However, the variability (**Supplementary Fig. 3**) and incomplete homogenization (**Supplementary Fig. 4**) suggested that the strong proteolysis of the original ExM protocol was necessary for reliable expansion.

We next sought to devise a strategy that would combine the convenience of direct protein anchoring with strong proteinase K treatment. It is known that GFP exhibits extraordinary stability to proteases[6,7]. We hypothesized that GFP and GFP-like FPs might retain their fluorescence after the proteolytic digestion required in the original ExM method, if they were retained in the polymer-specimen composite using AcX. We discovered that treatment with AcX followed by the standard ExM workflow, including proteinase K digestion, preserved GFP fluorescence in the expanded gel with high efficiency (65% ± 5% preservation; mean ± s.d.; $n = 4$; **Figs. 1a** and **2b**, and **Supplementary Fig. 5**). Because of the utility of this protocol, we termed the process of AcX treatment of a fixed specimen, followed by gelation, strong digestion, expansion and imaging as protein retention expansion microscopy (proExM).
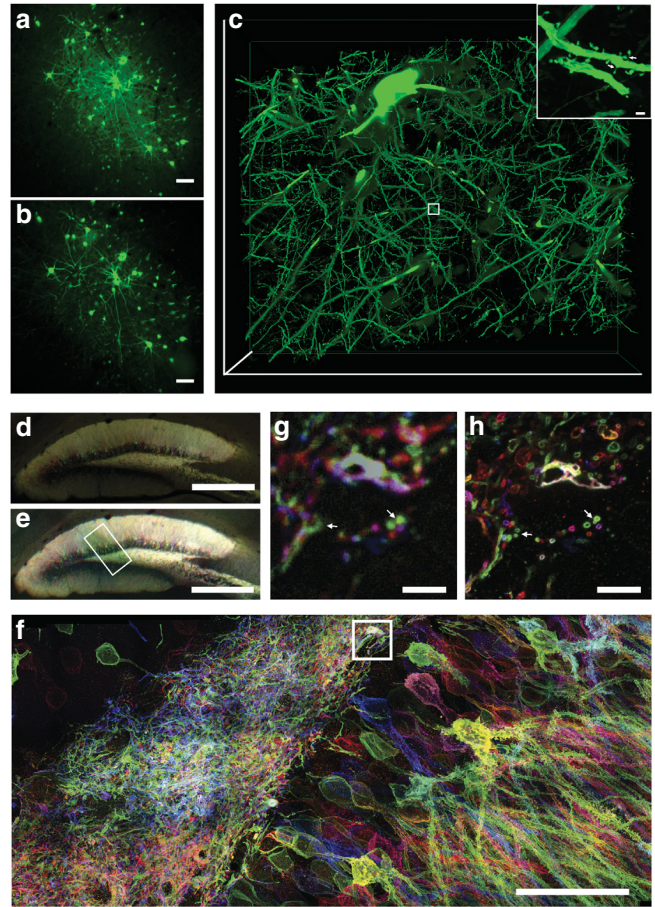
We systematically examined persistence of fluorescence for various FPs in the proExM workflow. We selected 20 widely used FPs with spectra ranging from the blue to the near-infrared

(**Supplementary Table 1**). We fused selected FPs to histone proteins and expressed them in human embryonic kidney (HEK293FT) cells. We compared images of live cultures vs. after-proExM images of the same cells (**Fig. 1a**). Most FPs retained more than 50% of their live fluorescence intensity after proExM ($n = 4$ samples each; **Fig. 1a,b** and **Supplementary Table 1**), which was comparable to the persistence of small-molecule fluorophores in the original ExM protocol[1].

Having seen that FPs could persist sufficiently to report signals even after a strong digestion process, we next sought to determine whether other signals might persist. We discovered that proExM anchors and preserves the fluorescence of, commercial fluorescently conjugated secondary antibodies. Following gelation and digestion, specimens labeled with secondary antibodies bearing a variety of small-molecule fluorophores retained ~50% of their initial brightness ($n = 3$ samples each; **Fig. 1c** and **Supplementary Table 2**). In the original ExM protocol, custom conjugation of secondary antibodies to enable labeling with a gel-anchorable fluorophore was required[1]. proExM allows commercial secondary antibodies to be used in place of those custom formulations.

In addition to antibodies, we also observed preservation of signals from fluorescently labeled streptavidin. Using streptavidin, we

Figure 3 proExM of mammalian brain circuitry. (**a,b**) Pre-expansion (**a**) and post-expansion (**b**) widefield image of GFP fluorescence in virally injected rhesus macaque cortex. (**c**) Volume rendering of confocal microscopy images of a subregion of **b**. Inset is a magnification of the boxed region, showing dendritic spines. (**d**) Low-magnification widefield fluorescence imaging showing immunostained mouse hippocampus expressing virally delivered Brainbow3.0. (**e**) Post-expansion widefield image of the sample in **e**. (**f**) Maximum intensity projection of high-resolution confocal microscopy stack following expansion of membrane labeled Brainbow3.0 neurons from the boxed region in **e**. (**g**) Pre-expansion confocal image showing one optical section of the boxed region in **f**. (**h**) Post-expansion image of **g**. Scale bars: (**a**) 100 μm, (**b**) 100 μm (physical size post-expansion, 413 μm), (**c**) 300 μm × 254 μm × 25 μm, (**c**) 1 μm, (**d**) 500 μm, (**e**) 500 μm (1,980 μm), (**f**) 5 μm, (**g**) 5 μm (19.8 μm), (**h**) 50 μm (198 μm).

imaged probes designed to capture cysteine S-nitrosation using a previously developed chemical method, SNOTRAP[8], thus demonstrating the imaging of S-nitrosation signals with proExM (**Supplementary Fig. 6**). This protocol also points toward the possibility of anchoring other protease-resistant tags to the polymer, followed by gelation, digestion, expansion and imaging, as a potentially generalized strategy.

Although the digestion step was the same as for our originally validated ExM protocol, suggesting that nanoscale isotropy would be preserved, we validated proExM by imaging immunostained microtubules in cultured cells with super-resolution structured illumination microscopy (SR-SIM) (**Fig. 1d**) before proExM and with confocal imaging after proExM (**Fig. 1e**), as we did to validate our original ExM protocol[1]. We quantified the root-mean-square (r.m.s.) error of feature measurements after proExM over length scales between 0 μm and 20 μm, and found that r.m.s. errors were ~1–2% of the measurement distance (**Fig. 1f**).

We performed proExM followed by confocal microscopy to image several fusion proteins bearing genetically encoded fluorophores (i.e., unstained) in cultured HeLa cells. We first examined fusions of tubulin, clathrin and keratin (**Fig. 1g–k**), which we and others have commonly used as stereotyped structures to demonstrate super-resolution imaging of cells[9–12]. The tubulin-mClover fusion presented a microtubule full-width at half-maximum (FWHM) of 67 nm ± 8 nm (*n* = 16 microtubules in three samples) (**Fig. 1h,i**), suggesting a resolution of better than 70 nm[11]. We also imaged clathrin-mEmerald in HeLa cells obtaining excellent definition of the nulls in the middle of the pits (**Fig. 1j**). Dual-color proExM imaging of fusion proteins containing mEmerald and mRuby2, two of the genetically encoded fluorophores in our screen, yielded excellent image quality as expected (keratin-mRuby2 and clathrin-mEmerald, **Fig. 1k**; paxillin-mEmerald and actin-mRuby2, **Fig. 1l**). We examined the stability of four photoswitchable FPs during proExM (**Supplementary Fig. 7** and **Supplementary Table 3**). We imaged cells expressing histone H2B-Dendra and mEos2-tubulin fusions with photoactivated localization microscopy (PALM) (**Supplementary Fig. 7**), demonstrating preservation of photoswitching fluorophores compatible with PALM (although validating resolution claims for post-ExM PALM is beyond the scope of this paper).

To assess the performance of proExM in various three-dimensional tissues, we performed proExM on four different mouse tissue types (brain, pancreas, lung and spleen, **Fig. 2a–d**). Mouse brain expressing YFP under the *Thy1* promoter (*Thy1-YFP*) in a sparse subset of neurons expanded without distortion at the millimeter scale after treatment with proteinase K as described for cultured cells (**Fig. 2a**). Pancreas, spleen and lung have different mechanical properties than brain (for example, more connective tissue), which hinders expansion after room-temperature proteinase K digestion. We antibody-stained

the intermediate filament vimentin as a marker of connective tissue to examine the isotropy of expansion in these diverse tissue types. We observed that, with a slight modification in the digestion temperature to the optimum of the proteinase K enzyme (60 °C for 4 h), proExM allowed for expansion of pancreas, lung and spleen tissue, with excellent preservation of tissue morphology at the millimeter length scale (**Fig. 2b–d**). High-resolution diffraction-limited microscopy of the tissue before (**Fig. 2e,f**) vs. after (**Fig. 2e,g**) proExM showed the resolution improvement with proExM. We quantified the isotropy of expansion by measuring the r.m.s. error of feature measurements after proExM at the microscale (<100 μm) for pancreas, lung and spleen tissue. The r.m.s. errors were small (1–3% of the measurement distance) and similar among all three of the tissue types (**Fig. 2h**) at this length scale.

To examine the isotropy of expansion at the nanoscale, we performed SR-SIM (**Fig. 2i,j**) and proExM confocal imaging (**Fig. 2i,k**) on vimentin staining in the pancreas. Again we observed small r.m.s. errors on the order of 1–5% of the measurement length for measurements between 0 μm and 25 μm (**Fig. 2l**; *n* = 4 fields of view from two samples). We performed a similar analysis on mouse brain cortical tissue stained with antibodies against Tom20, a mitochondrial marker, and imaged with SR-SIM before (**Fig. 2m,n**) and confocal microscopy after (**Fig. 2o**) proExM processing using proteinase K digestion at room temperature. R.m.s. errors for this tissue type were 1–3% of the measurement length, between 0 μm and 40 μm (**Fig. 2p**, *n* = 3 specimens).

Transgenic animals expressing FPs, as well as animals expressing FPs after viral gene delivery, are routinely used in biology for labeling proteins and cells in intact tissues and organisms. We applied proExM
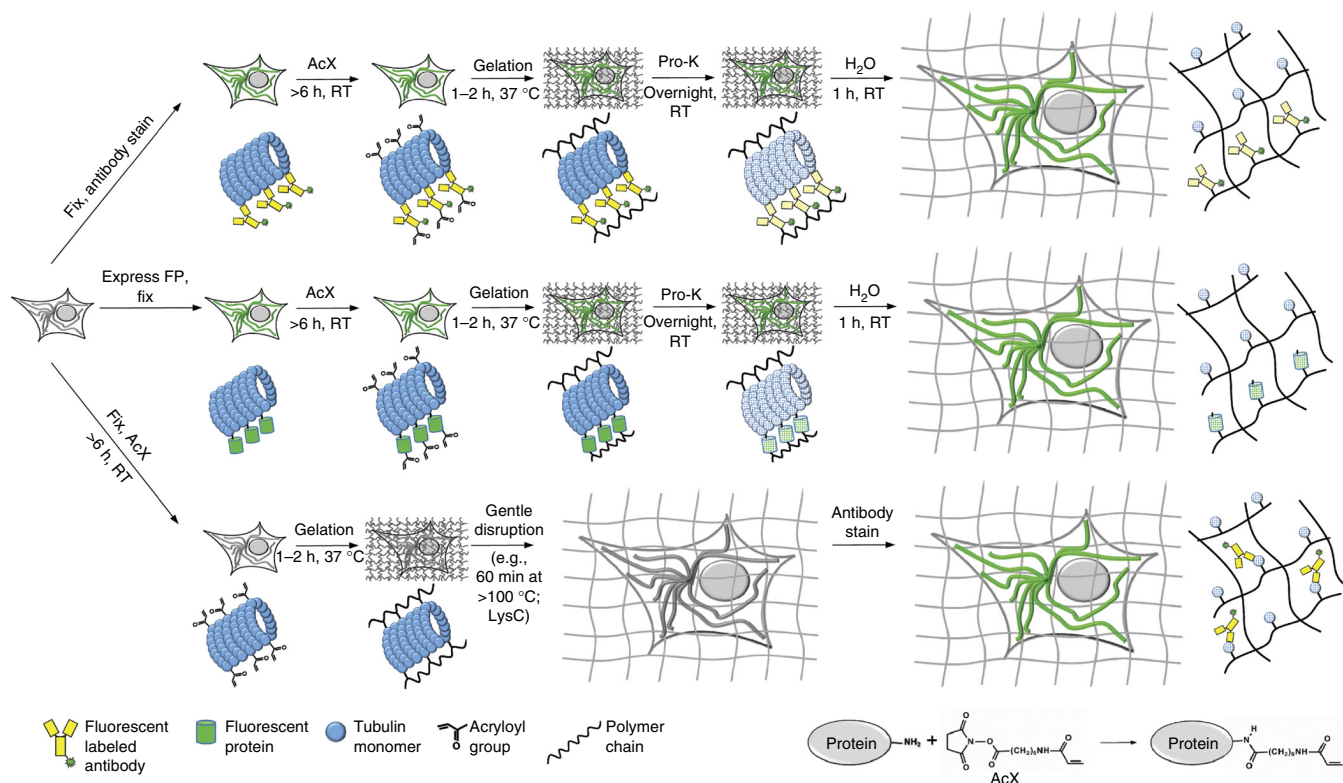
Figure 4 Three workflows for expansion microscopy with protein retention. Samples are chemically fixed and stained with antibodies, using conventional immunostaining protocols, before AcX treatment at room temperature (RT) and subsequent ExM processing (gelation, proteinase K treatment and expansion in water; top). Samples expressing FPs are chemically fixed (and optionally permeabilized) before AcX treatment and subsequent ExM processing (middle). Samples treated with AcX, followed by gelation, are then processed with a gentle homogenization procedure (for example, alkaline hydrolysis and denaturation, or digestion with LysC), and finally antibody staining in the expanded state (bottom).

for visualization of FPs expressed in intact mammalian brain tissue, including the brains of mice (**Supplementary Fig. 8**) and a rhesus macaque (**Fig. 3a–c**), obtaining images that showed minimal macroscale distortion after expansion (**Fig. 3a,b**). Using a high-magnification lens on a conventional confocal microscope, dendritic spine morphology was easily resolved after expansion, with even thin spine necks visible (**Fig. 3c**).

We applied proExM for imaging of mouse brain circuitry expressing virally delivered Brainbow3.0 (refs. 13,14), which marks neurons with random combinations of membrane-anchored FPs. These FPs are antigenically distinct to allow for subsequent amplification via antibodies. Following proExM, antibody staining and morphology were preserved in brain tissues (**Fig. 3d,e**). Confocal imaging allowed for large volume, multicolor super-resolved imaging of the Brainbow sample (**Fig. 3f**). Side-by-side comparison of confocal images before and after expansion showed how axons and dendrites too close to resolve before expansion can be clearly resolved after expansion (**Fig. 3g,h**).

We here report that it is possible to directly anchor proteins to a swellable gel synthesized throughout a biological sample, by applying a commercially available small molecule cross-linker before gelation. This proExM strategy can be used to perform nanoscale imaging of immunostained cells and tissues as well as samples expressing various FPs (**Fig. 4**). ProExM variants can support post-expansion antibody delivery, potentially increasing brightness of staining and antibody access (**Fig. 4**).

We showed that native proteins anchored in this way can retain epitope functionality and be labeled after expansion if the nonspecific

proteolysis of ExM is replaced with modified post-gelation homogenization treatments. Such approaches may overcome the limitations inherent to delivering antibodies in the crowded environment of native tissue[15–19]. For example, closely packed epitopes may bind antibodies poorly in dense tissue but better access antibodies after expansion (**Supplementary Fig. 1**).

We found that FPs and fluorescent antibodies delivered using standard methods are also retained in the gel, and furthermore exhibit fluorescence signals after nonspecific proteolysis treatment. We demonstrated the multicolor, large-volume capability of proExM by expanding Brainbow samples, which may be useful for circuit mapping. ProExM is simple and easily integrated into existing sample workflows. Preservation of endogenous fluorescence allows for the use of transgenic animals, viral expression vectors and transfection of FP constructs, all without immunostaining.

As with our original ExM protocol, samples processed with proExM are optically clear and index-matched to water[1]. This allows for super-resolution imaging deep into samples, on conventional fluorescence microscopes, limited only by working distance of the objective lens. As an effective subdiffraction-limited imaging modality, ExM protocols exhibit great speed of imaging. Although samples prepared by ExM protocols are larger in size than before expansion (and thus may require longer working distance objectives and tiled acquisition), there is a net win, as ExM protocols enable voxel sizes of super-resolution microscopy with imaging at voxel acquisition rates of conventional microscopy. Like ExM, proExM does not require specialized hardware, extensive post-processing or other enabling aspects of conventional super-resolution methods. As with any super-resolution

method, because voxels are smaller, they contain fewer fluorophores and are thus dimmer than unexpanded specimens. This effect is offset by the concomitant dilution of autofluorescence and reduced loss owing to scattering, though longer exposure times are typically useful, depending on the brightness of the unexpanded specimen. proExM physically magnifies samples equally well along the axial as well as lateral dimensions. Expanded samples are compatible with downstream imaging and analysis strategies such as tomography, deconvolution or even traditional super-resolution imaging (for example, PALM, as shown here). Thus proExM will likely find many applications in supporting routine imaging of complex biological samples with nanoscale precision.

METHODS

Methods and any associated references are available in the online version of the paper.

Note: Any Supplementary Information and Source Data files are available in the online version of the paper

AUTHOR CONTRIBUTIONS

P.W.T., F.C., K.D.P., Y.Z., C.-C.Y. and E.S.B. all contributed key ideas, analyzed data and wrote the paper. P.W.T. designed and performed antigen retrieval experiments. F.C. designed and performed AcX-secondary antibody retention experiments and Brainbow experiments. K.D.P. and F.C. designed and performed fluorophore preservation experiments. Y.Z. designed and performed LysC experiments. C.-C.Y. and P.W.T. designed and performed depth modulation of AcX experiments and preliminary characterizations of autoclave treatments. L.G. created code for data analysis. B.P.E. carried out PALM experiments. A.M. and H.-J.S. carried out mouse surgeries. F.Y. carried out primate surgeries under the supervision of R.D. with assistance from E.M.D. D.H.R. and D.C. assisted with Brainbow experiment design. G.G., U.S. and S.R.T. designed and performed the SNOTRAP experiment. F.C. and Y.Z. designed and performed experiments for validation of proExM on non-brain mouse tissue. E.S.B. supervised the project.

COMPETING FINANCIAL INTERESTS

The authors declare competing financial interests: details are available in the online version of the paper.

Reprints and permissions information is available online at http://www.nature.com/reprints/index.html.

1. Chen, F., Tillberg, P.W. & Boyden, E.S. Optical imaging. Expansion microscopy. *Science* **347**, 543–548 (2015).
2. Laemmli, U.K. Cleavage of structural proteins during the assembly of the head of bacteriophage T4. *Nature* **227**, 680–685 (1970).
3. Hunt, N.C., Attanoos, R. & Jasani, B. High temperature antigen retrieval and loss of nuclear morphology: a comparison of microwave and autoclave techniques. *J. Clin. Pathol.* **49**, 767–770 (1996).
4. Jekel, P.A., Weijer, W.J. & Beintema, J.J. Use of endoproteinase Lys-C from Lysobacter enzymogenes in protein sequence analysis. *Anal. Biochem.* **134**, 347–354 (1983).
5. Wu, C.C., MacCoss, M.J., Howell, K.E. & Yates, J.R. III. A method for the comprehensive proteomic analysis of membrane proteins. *Nat. Biotechnol.* **21**, 532–538 (2003).
6. Sniegowski, J.A., Phail, M.E. & Wachter, R.M. Maturation efficiency, trypsin sensitivity, and optical properties of Arg96, Glu222, and Gly67 variants of green fluorescent protein. *Biochem. Biophys. Res. Commun.* **332**, 657–663 (2005).
7. Bokman, S.H. & Ward, W.W. Renaturation of Aequorea gree-fluorescent protein. *Biochem. Biophys. Res. Commun.* **101**, 1372–1380 (1981).
8. Seneviratne, U. *et al.* S-nitrosation of proteins relevant to Alzheimer's disease during early stages of neurodegeneration. *Proc. Natl. Acad. Sci. USA* **113**, 4152–4157 (2016).
9. Huang, B., Jones, S.A., Brandenburg, B. & Zhuang, X. Whole-cell 3D STORM reveals interactions between cellular structures with nanometer-scale resolution. *Nat. Methods* **5**, 1047–1052 (2008).
10. Rego, E.H. *et al.* Nonlinear structured-illumination microscopy with a photoswitchable protein reveals cellular structures at 50-nm resolution. *Proc. Natl. Acad. Sci. USA* **109**, E135–E143 (2012).
11. Bates, M., Huang, B., Dempsey, G.T. & Zhuang, X. Multicolor super-resolution imaging with photo-switchable fluorescent probes. *Science* **317**, 1749–1753 (2007).
12. Bossi, M. *et al.* Multicolor far-field fluorescence nanoscopy through isolated detection of distinct molecular species. *Nano Lett.* **8**, 2463–2468 (2008).
13. Cai, D., Cohen, K.B., Luo, T., Lichtman, J.W. & Sanes, J.R. Improved tools for the Brainbow toolbox. *Nat. Methods* **10**, 540–547 (2013).
14. Livet, J. *et al.* Transgenic strategies for combinatorial expression of fluorescent proteins in the nervous system. *Nature* **450**, 56–62 (2007).
15. Schnell, U., Dijk, F., Sjollema, K.A. & Giepmans, B.N.G. Immunolabeling artifacts and the need for live-cell imaging. *Nat. Methods* **9**, 152–158 (2012).
16. Hackstadt, T. Steric hindrance of antibody binding to surface proteins of Coxiella burnetti by phase I lipopolysaccharide. *Infect. Immun.* **56**, 802–807 (1988).
17. Jiménez, N. & Post, J.A. A novel approach for intracellular 3D immuno-labeling for electron tomography. *Traffic* **13**, 926–933 (2012).
18. Randall, K.J. & Pearse, G. A dual-label technique for the immunohistochemical demonstration of T-lymphocyte subsets in formalin-fixed, paraffin-embedded rat lymphoid tissue. *Toxicol. Pathol.* **36**, 795–804 (2008).
19. Kakimoto, K., Takekoshi, S., Miyajima, K. & Osamura, R.Y. Hypothesis for the mechanism for heat-induced antigen retrieval occurring on fresh frozen sections without formalin-fixation in immunohistochemistry. *J. Mol. Histol.* **39**, 389–399 (2008).

ONLINE METHODS

Fluorescent protein screening. Most of the mammalian plasmids were obtained from Addgene (**Supplementary Tables 1** and **3**). To construct the remaining ones, pmKate2-H2B-N1 and pPATagRFP-H2B-N1 plasmids the respective genes were PCR-amplified as AgeI/NotI fragments and swapped with the LSSmOrange gene in pH2B-LSSmOrange-N1 (Addgene). To generate NLS-iRFP fusion protein, a PCR-amplified AgeI/NotI fragment encoding gene of iRFP was swapped with LSSmKate2 gene in pNLS-LSSmKate2-N1 (Addgene plasmid 31871). HEK293FT (Invitrogen) and HeLa (ATCC CCL-2) cells were cultured in DMEM (Cellgro) supplemented with 10% FBS (Invitrogen), 1% penicillin/streptomycin (Cellgro), and 1% sodium pyruvate (BioWhittaker). HEK293FT and HeLa cells were used for ease of transfection; cell lines were authenticated by STR profiling and checked for mycoplasma contamination by the manufacturer. Cells were transfected using TransIT-X2 transfection reagent (Mirus Bio) according to the manufacturer's protocol. Widefield imaging of live HEK293FT cells was performed 24 h after transfection using a Nikon Eclipse Ti inverted microscope equipped with $10 \times$ NA 0.3 objective lens, a SPECTRA X light engine (Lumencor) with 390/22 nm, 438/24 nm, 475/28 nm, 510/25 nm, 585/29 nm, and 631/28 nm exciters (Semrock), and a 5.5 Zyla camera (Andor), controlled by NIS-Elements AR software. Immediately after live-cell imaging, cell cultures were fixed with 4% paraformaldehyde for 10 min, and permeabilized with 0.1% Triton-X for 15 min, washed three times for 5 min with phosphate-buffered saline (PBS; Cellgro) and treated with 0.1 mg/ml AcX (Life Technologies) for at least 6 h, gelled and digested with proteinase K overnight as described below.

Following digestion, the samples were processed by extensively washing with PBS, and then shrunk in 1 M NaCl and 60 mm $MgCl_2$ (except for YFP, which is chloride-sensitive[20], and thus was measured in the expanded state). For control experiments shown in **Supplementary Figure 5** gels were washed only with PBS. Registration of pre- and post-sample processing images was carried out with an implementation of the SIFT/RANSAC algorithm, in Matlab. Automatic Otsu thresholding via CellProfiler[21] of fluorescent nuclei allowed for automated measurement of fluorescence intensity in the same set of cells before and after sample processing. Intensity measurements for each nucleus before and after sample processing were normalized by segmented area to account for fluorophore dilution (area was used since epifluorescence optical sectioning mitigates the axial expansion effect on brightness).

Quantification of fluorescent dye retention during ProExM. Fluorescent secondary antibodies (goat anti-rabbit, 10 μg/mL) were purchased from commercial vendors (see **Supplementary Table 2** for list of fluorescent secondary antibodies). Retention (**Fig. 1c**) was quantified via before-after proExM imaging mouse cortex as described below. Cortical sections of wild type (only used for Alexa Fluor 488 owing to Thy1-YFP cross-talk) and Thy1-YFP brain slices (50 μm thick) were stained with anti-Homer primary antibody (Synaptic Systems; **Supplementary Table 4**), and different secondary antibodies described in **Supplementary Table 2**. Epifluorescence images of brain slices were taken with 4×0.13 NA objective pre-gelation. Following proExM gelation and digestion, the brain slices were washed extensively with PBS (3×30 min), and epifluorescence images of the slice were taken again with identical imaging conditions. A region of interest in the cortex was used to determine the loss of fluorescence during proExM processing. Intensity measurements before and after sample processing were normalized by segmented area to account for fluorophore dilution.

Structured illumination microscopy pre-expansion imaging. HeLa cells were fixed with 4% paraformaldehyde for 10 min, washed three times for 5 min with PBS, and permeabilized with 0.1% Triton-X for 15 min. Microtubules in fixed HeLa were stained with primary antibodies (Sheep Anti-Tubulin, Cytoskeleton ATN02) in blocking buffer $1 \times$ PBS with 0.1% Triton X-100 and 2% normal donkey serum (PBT) at a concentration of 10 μg/mL for 1–4 h and then washed in PBS three times for 5 min each. Specimens were then incubated with secondary antibodies (donkey anti-sheep Alexa Fluor 488, Life Technologies, 10 μg/mL) in PBT for 1–4 h and then washed in PBS three times for 5 min. 50-μm brain tissue slices were prepared and stained with primary and secondary antibodies (Rabbit Anti-Tom20, Santa Cruz Biotech sc-11415

and goat anti-rabbit Alexa Fluor 568 (Life Technologies)) as described below. SR-SIM imaging was performed on a Deltavision OMX Blaze (GE healthcare) SIM microscope with 100×1.40 NA (Olympus) oil objective. Stained cells were imaged with SlowFade Gold (Invitrogen) antifade reagent for suppression of photobleaching and refractive index matching for pre-expansion imaging.

Measurement error quantification. The same fields of view were imaged before and after expansion. Post-expansion images were first registered to the corresponding pre-expansion images by rotation, translation and uniform scaling. In case the specimen tilt changed between pre- and post-expansion imaging, this was corrected using a 3D rotation without scaling using the Fiji 3D Viewer package. These scaled images were then registered again to the pre-expansion images, but this time with a B-spline-based non-rigid registration package in Matlab[22] to capture any non-uniformities in the expansion process. Control points for registration were automatically generated using scale-invariant feature transform (SIFT) keypoints[23]. SIFT keypoints were generated using the VLFeat open source library[24], and random sample consensus (RANSAC) was used to estimate a geometric transformation limited to rotation, translation and scaling. The vector deformation field mapping the scaled post-expansion image to the pre-expansion image expresses the shift of each point in the post-expansion image relative to an ideal uniform expansion. By subtracting the resulting vectors at any two points, we found the relative localization error in using the post-expansion image to measure the distance between those two points. We sampled the entire population of possible point-to-point measurements and found the r.m.s. error for such measurements as a function of measurement length.

Brainbow3.0 injection and antibody staining. Brainbow3.0 rAAV (University of Pennsylvania, Penn Vector Core) injections were performed as previously described[13]. Briefly, transgenic mice (Emx1-Cre) were anesthetized continuously with isoflurane and head-fixed to a stereotaxic apparatus. Surgery took place under sterile conditions with the animal lying on a heating pad. 2 μL AAV mix (7.5×10^{12} genome copy/mL) was injected at a rate of 0.2 μl/min through a 34-gauge injection needle into the brain (for example, cortex, hippocampus), after which the needle was allowed to rest at the injection site for 5 min to allow viral diffusion. Animals expressed virus for 3–4 weeks and then were perfused (see below).

Primary antibodies against Brainbow 3.0 fluorophores (chicken anti-GFP, guinea-pig anti-mKate2, rat anti-mTFP) were produced by the Cai laboratory, University of Michigan Medical School, Ann Arbor, Michigan, USA. Slices were permeabilized and blocked with $1 \times$ PBS with 0.1% Triton X-100 and 2% normal donkey serum (PBT) for 30 min before antibody staining (all incubations at room temperature (RT)). Slices were incubated with primary antibodies for 3 d at 4 °C in PBT, and then washed four times 30 min with PBT. Slices were incubated with secondary antibodies for 1 d at RT. Secondary antibodies used were: goat anti-chicken Alexa Fluor 488, goat anti-rat Alexa Fluor 546 (Life Technologies) and donkey anti-guinea pig CF633 (Biotium), all at 10 μg/ml.

Mouse perfusion. All solutions below were made up in $1 \times$ PBS. Mice were anesthetized with isoflurane and perfused transcardially with ice-cold 4% paraformaldehyde. Brains were dissected, left in 4% paraformaldehyde at 4 °C for 1 d, before being moved to 100 mM glycine. Slices (50 μm and 100 μm) were sliced on a vibratome (Leica VT1000S) and stored at 4 °C until staining.

AcX treatment. Acryloyl-X, SE (6-((acryloyl)amino)hexanoic acid, succinimidyl ester; here abbreviated AcX; Thermo-Fisher) was resuspended in anhydrous DMSO at a concentration of 10 mg/mL, aliquoted and stored frozen in a desiccated environment. AcX prepared this way can be stored for up to 2 months. For anchoring, cells and tissue slices are incubated in AcX diluted in PBS at a concentration of 0.1 mg/mL for >6 h, at RT. For thick tissue (>100 μm), AcX penetration depth and labeling uniformity can be improved by incubating the sample at lower pH, at lower temperature, and in a 2-(*N*-morpholino)ethanesulfonic acid (MES)-based saline (100 mM MES, 150 mM NaCl; **Supplementary Fig. 9**). Tissue slices can be incubated on a shaker or rocker to ensure mixing during the reaction.

Gelation, digestion and expansion. For AcX-anchored FPs and antibody staining, the following steps (gelation, digestion and expansion) were performed as described previously[1]. Briefly, monomer solution (1 × PBS, 2 M NaCl, 8.625% (w/w) sodium acrylate, 2.5% (w/w) acrylamide, 0.15% (w/w) N,N'-methylenebisacrylamide) was mixed, frozen in aliquots, and thawed before use. Monomer solution was cooled to 4 °C before use. Concentrated stocks (10% w/w) of ammonium persulfate (APS) initiator and tetramethylethylenediamine (TEMED) accelerator were added to the monomer solution up to 0.2% (w/w) each. For slices, the inhibitor 4-hydroxy-2,2,6,6-tetramethylpiperidin-1-oxyl (4-hydroxy-TEMPO) was added up to 0.01% (w/w) from a 0.5% (w/w) stock to inhibit gelation during diffusion of the monomer solution into tissue sections. Cells or tissue slices were incubated with the monomer solution plus APS/TEMED (and 4-hydroxy-TEMPO for slices) at 4 °C for 1 min, 30 min for cultured cells, and brain slices, respectively, and then transferred to a humidified 37 °C incubator for 2 h for gelation.

Proteinase K (New England BioLabs) was diluted 1:100 to 8 units/mL in digestion buffer (50 mM Tris (pH 8), 1 mM EDTA, 0.5% Triton X-100, 1 M NaCl) and incubated with the gels fully immersed in proteinase solution overnight at RT (this step can also be performed at 37 °C for 4 h). Digested gels were next placed in excess volumes of doubly deionized water for 0.25–2 h to expand, with longer times for thicker gels. This step was repeated 3–5 times in fresh water, until the size of the expanding sample plateaued.

Fluorescence microscopy after expansion. Post-expansion confocal imaging of cells was performed on an Andor spinning disk (CSU-X1 Yokogawa) confocal system with a 60 × 1.40 NA oil objective (**Fig. 1**). To quantify expansion factor for tissue slices and low-magnification before vs. after comparisons, specimens were imaged pre-ExM on a Nikon Ti-E epifluorescence microscope with a 4 × 0.13 NA air objective (**Fig. 2a–d**, and **Supplementary Figs. 1a,b, 3b, 5a–g** and **8a,b**). For data in **Figure 3a,b**, tissue slices were imaged on Nikon Ti-E epifluorescence microscope with a 10 × 0.45 NA. Otherwise, all other tissues presented were imaged using an Andor spinning disk (CSU-X1 Yokogawa) confocal system with a 40 × 1.15 NA water immersion objective (Nikon) with the exception of **Supplementary Figures 1, 3a, 4** and **6**, where a Zeiss LSM 710 with 40 × 1.1 NA water objective. The Zeiss LSM 710 with 10 × 0.3 NA air lens was used for **Supplementary Figure 9i**.

To stabilize the gels against drift during imaging following expansion, gels were placed in glass-bottom six-well plates with all excess liquid removed. If needed for immobilization, liquid low-melt agarose (2% w/w) was pipetted around the gel and allowed to solidify, to encase the gels before imaging.

PALM imaging. PALM data were recorded on a custom-built three-camera RAMM frame microscope (ASI) using an Olympus 1.4 NA PLAPON 60 × OSC objective, and a custom tube lens (LAO-300.0, Melles Griot), resulting in 100 × overall magnification[25]. A 2-mm-thick quad-band excitation dichroic (ZT405/488/561/640rpc, Chroma), a 2-mm-thick emission dichroic (T560lpxr, Chroma), and a band-pass emission filter (FF01-609/54-25, Semrock) filtered the emitted light. Dendra2 was photoconverted by 100 µs long excitation pulses of 405 nm (50 W/cm^2) every 200 ms, which was ramped up to 1.2 ms pulses every 200 ms during the course of image acquisition. Stroboscopic 405-nm excitation of the Stradus 405-100 laser (Vortran) was achieved using a NI-DAQ-USB-6363 acquisition board (National Instruments), Photoconverted Dendra2 molecules were excited with a 555-nm DPSS laser (CrystaLaser) at estimated sample power levels of 2 kW/cm^2. Fluorescence was detected using µManager (v. 1.4.20)[26] with a back-illuminated EMCCD camera (Andor Technology, Ixon Ultra DU-897_BV, 17 MHz EM amplifier, Gain 500, full-chip) at 20 frames/s.

Particle localization. Localizer[27] was used for eight-way adjacency particle detection with 20 GLRT sensitivity and a PSF of 1.3 pixels. The resulting particles were drift corrected using *ad hoc* fiducial markers. For each detected particle, integrated fluorescence intensities were converted to photon counts using analysis routines written in Igor Pro version 6.36. The mean and median localization errors were determined using equation (6) in ref. 28.

ProExM of different tissue types. Standard histology preparations of mouse normal fresh-frozen tissue sections, postfixed with cold acetone, of pancreas, spleen and lung (5–10 µm) were obtained from US Biomax (MOFTS036,

MOFTS051, and MOFTS031, respectively). Tissues were blocked with 1 × PBS with 0.1% Triton X-100 and 2% normal donkey serum (PBT) for 30 min before antibody staining. Tissues were stained with primary chicken anti-vimentin (Abcam) for 4 h at RT and then washed four times 30 min with PBT. Slices were incubated with secondary antibodies for 2 h at RT (anti-chicken Alexa Fluor 488, Life Technologies). Pre-expansion imaging was performed as described above. Tissues were incubated with 0.05 mg/mL AcX in PBS at RT overnight before gelation, digestion and expansion described above with the exception that digestion was performed at 60 °C for 4 h.

Antibody staining of endogenous proteins. Specimens, either before gelation or after autoclave or LysC treatment, were incubated in 1 × PBS with 0.1% Triton X-100 and 2% normal donkey serum (PBT) at RT for 2 h for blocking, and in the case of pre-gelation specimens, permeabilization. Specimens were incubated with primary antibodies (**Supplementary Table 4**) at 3 µg/mL in PBT, for 4 h (RT), and then washed four times 30 min with PBT. Specimens were incubated with secondary antibodies at 20 µg/mL in PBT, for 4 h (RT), and then washed four times at least 30 min with PBT. Secondary antibodies used were: goat anti-chicken Alexa Fluor 488 (Life Technologies), goat anti-rabbit Alexa Fluor 546 (Life Technologies) and goat anti-mouse CF633 (Biotium), except that goat anti-chicken Alexa Fluor 546 (Life Technologies) was used for experiments shown in **Supplementary Figure 1e,g,h** and goat anti-rabbit Alexa Fluor 488 (Life Technologies) was used for experiments shown in **Figure 1e**.

Specimen disruption using autoclave. After gelation, gels were recovered from gelation chambers and washed in 1 M NaCl. Gels were washed for 15 min in disruption buffer (100 mM Tris base, 5% Triton X-100, 1% SDS), then placed in fresh disruption buffer and treated by autoclave on liquid sterilization mode with a temperature of 121 °C held for 1 h. This treatment must be carried out in an autoclave-safe vessel such as polypropylene tubes. Gels were then transferred to well plates for antibody staining and imaging and washed in PBT (1 × PBS, 2% normal donkey serum, 0.1% Triton X-100) to remove disruption buffer.

Mild digestion with LysC. After gelation, gels were pre-treated in HBSS buffer (with calcium and magnesium, ThermoFisher Scientific) with 600 U/ml collagenase type II (Life Technologies) in 37 °C for 2–4 h. Gels were then washed for 5 min in LysC digestion buffer (25 mM Tris-HCl, 1 mM EDTA, pH 8.5) and incubated with 33 µg/ml LysC (Promega) in 37 °C for at least 8 h. Finally, gels were washed in LysC digestion buffer 3 × for 30 min each and were subjected to immunostaining with identical steps to those described above.

Synthesis of SNOTRAP-biotin. To a stirred 2-(diphenylphosphino)-benzenethiol (100 mg, 0.34 mmol) in dry DMF (5 mL) was added biotin-PEG$_3$-propionic acid (100 mg, 0.22 mmol, ChemPep, Inc,), N,N'-dicyclohexylcarbodiimide (DCC) (70 mg, 0.34 mmol) and dimethylaminopyridine (DMAP) (4 mg, 0.03 mmol) successively. The resulting mixture was stirred for 7 h at RT, and the resulting clear solution then concentrated under reduced pressure and purified by flash chromatography (hexane/EtOAc/MeOH gradient) to give the desired product (yield 30%). The SNOTRAP probe was repurified on an 1100 HPLC system with a photodiode array UV detector at 254 nm (Agilent Technologies). HPLC columns and solvent systems were as follows: a semi-preparative Phenomenex Luna C18 (25 cm × 9.4 mm, 10 µm) column was eluted with a linear gradient of 0.1% formic acid in water (A) and acetonitrile (B) at a flow rate of 2.5 mL/min. Solvent composition was initially at 40% for 5 min, 70% at 10 min, 90% at 20 min, and then further to 95% B over 8 min. ^{1}H NMR (500 MHz, CD$_3$CN, δ) 7.42–7.38 (m, 9H), 7.23–7.18 (m, 4H), 7.84 (m, 1H), 4.60–4.51 (m, 2H), 3.67–3.51 (m, 12H), 3.2 (m, 3H), 2.8 (m, 2H), 2.55 (t, 2H), 2.15 (t, 2H), 1.57-3.51 (m, 6H); ^{13}C NMR (125 MHz, CD$_3$CN, δ) 199.19, 172.5, 164.5, 144.8, 138.1, 137.0, 134.8, 129.9, 129.6, 129.6, 118.3, 69.2, 63.1, 62.3, 45.9, 42.5, 38.2, 27.1, 23.1, 22.5; ^{31}P NMR (202 MHz, CD$_3$CN, δ) −10.3; HRMS-ESI$^+$ (m/z): [M + H]$^+$ calculated for C$_{37}$H$_{47}$N$_3$O$_6$PS$_2$, 724.2638; found, 724.2632.

ProExM of SNOTRAP staining. For SNOTRAP staining, primary neuron culture were washed 3 × 5 min using PBS and fixed using cold methanol at

−20 °C for 15 min. Neurons were incubated with 300 nM N-ethylmaleimide (NEM) (Thermo Scientific) in PBS containing Triton X-100 (0.3% v/v) at 37 °C for 30 min to block the free –SH group on proteins. Cells were then washed 3 × 5 min using PBS and incubated with SNOTRAP probe (250 µM) in acetonitrile-PBS-triton (50%:50% v/v) at RT for 1 h, and then further incubated with streptavidin-Alexa Fluor 488 (Thermo Scientific) in 1/500 dilution (PBS-Triton) at RT for 1 h and afterward washed 5 × 5 min. Antibody staining for anti-tubulin (Alexa Fluor 546 secondary antibody) and proExM was performed as described above.

Animal care. All methods for animal care and use were approved by the Massachusetts Institute of Technology Committee on Animal Care and were in accordance with the National Institutes of Health Guide for the Care and Use of Laboratory Animals. One adult male rhesus macaque (*Macaca mulatta*) weighing 12 kg was used for this study, as well as 1 C57BL/6 mouse, 4 Emx1-Cre mice, and 10 Thy1-YFP mice, ages ~1–3 months old. Mice were used without regard for gender.

Macaque procedures. Virus injections were performed with sevoflurane anesthesia using stereotactic coordinates to target eight injection sites. Viruses (AAV8) were centrifuged and loaded into 10 µL gas-tight syringes (Hamilton) that had been back-filled with silicone oil (Sigma). A total of 3 µL of virus was infused into the brain at two locations (deep then 500 µm superficial) at a rate of 100–200 nL/min using stereotactic micromanipulator arms (David Kopf Instruments) and UMP3 micro-syringe injector pumps (World Precision Instruments). After each injection, the needle and syringe were left in place for 10 min before withdrawal. Blunt 33G needles were used for all injections.

1 mg dexamethasone was also administered to prevent brain swelling. The animal was killed 4 weeks after viral injection. An overdose of pentobarbital was administered before perfusion with PBS and 4% paraformaldehyde. The brain was then extracted, blocked, stored in a 20% glycerol with 0.1% sodium azide solution, and finally cut into 40-µm microtome sections.

20. Wachter, R.M. & Remington, S.J. Sensitivity of the yellow variant of green fluorescent protein to halides and nitrate. *Curr. Biol.* **9**, R628–R629 (1999).
21. Carpenter, A.E. *et al.* CellProfiler: image analysis software for identifying and quantifying cell phenotypes. *Genome Biol.* **7**, R100 (2006).
22. Kroon, D.-J. B-splineGrid Image and Point based Registration. *Matlab Cent.* at http://www.mathworks.com/matlabcentral/fileexchange/20057-b-spline-grid–image-and-point-based-registration.
23. Lowe, D.G. Distinctive image features from scale-invariant keypoints. *Int. J. Comput. Vis.* **60**, 91–110 (2004).
24. Vedaldi, A. & Fulkerson, B. Vlfeat. *Proc. Int. Conf. Multimed. – MM* 1469 (ACM Press, 2010).
25. English, B.P. & Singer, R.H. A three-camera imaging microscope for high-speed single-molecule tracking and super-resolution imaging in living cells. *SPIE Nanosci. + Eng.* (eds. Mohseni, H., Agahi, M.H. & Razeghi, M.) 955008 (International Society for Optics and Photonics, 2015).
26. Edelstein, A., Amodaj, N., Hoover, K., Vale, R. & Stuurman, N. Computer control of microscopes using µManager. *Curr. Protoc. Mol. Biol.* Chapter 14, Unit 14.20 (2010).
27. Dedecker, P., Duwé, S., Neely, R.K. & Zhang, J. Localizer: fast, accurate, open-source, and modular software package for superresolution microscopy. *J. Biomed. Opt.* **17**, 126008 (2012).
28. Mortensen, K.I., Churchman, L.S., Spudich, J.A. & Flyvbjerg, H. Optimized localization analysis for single-molecule tracking and super-resolution microscopy. *Nat. Methods* **7**, 377–381 (2010).